Nuclear Engineering and Technology 48 (2016) 1–15

Available online at ScienceDirect

Nuclear Engineering and Technology

journal homepage: www.elsevier.com/locate/net

Invited Article

Development Status of Accident-tolerant Fuel for Light Water Reactors in Korea

Hyun-Gil Kim [a,*], *Jae-Ho Yang* [a], *Weon-Ju Kim* [b], *and Yang-Hyun Koo* [a]

[a] *LWR Fuel Technology Division, Korea Atomic Energy Research Institute, 989-111 Daedeok-daero, Yuseong-gu, Daejeon 34057, South Korea*
[b] *Nuclear Materials Development Division, Korea Atomic Energy Research Institute, 989-111 Daedeok-daero, Yuseong-gu, Daejeon 34057, South Korea*

ARTICLE INFO

Article history:
Received 11 December 2015
Accepted 11 December 2015
Available online 23 December 2015

Keywords:
Accident-Tolerant Fuel
Fukushima Accident
Microcell Fuel Pellet
SiC Composite Cladding
Surface-Modified Cladding

ABSTRACT

For a long time, a top priority in the nuclear industry was the safe, reliable, and economic operation of light water reactors. However, the development of accident-tolerant fuel (ATF) became a hot topic in the nuclear research field after the March 2011 events at Fukushima, Japan. In Korea, innovative concepts of ATF have been developing to increase fuel safety and reliability during normal operations, operational transients, and also accident events. The microcell UO_2 and high-density composite pellet concepts are being developed as ATF pellets. A microcell UO_2 pellet is envisaged to have the enhanced retention capabilities of highly radioactive and corrosive fission products. High-density pellets are expected to be used in combination with the particular ATF cladding concepts. Two concepts—surface-modified Zr-based alloy and SiC composite material—are being developed as ATF cladding, as these innovative concepts can effectively suppress hydrogen explosions and the release of radionuclides into the environment.

1. Introduction

The Fukushima earthquake in Japan generated serious issues concerning light water reactor (LWR) fuel performance under accident conditions. In severe nuclear power plant accidents, a large amount of radioactivity is released into the environment from the reactor containment. From the experience of the Fukushima accident, it was recognized that hydrogen explosions and the release of radionuclides can have a serious impact on the public [1]. These two problems—hydrogen explosion and release of radionuclides—are caused by the severe damage of current nuclear fuels, composed of fuel pellets and fuel cladding, during an accident.

Under the high-temperature steam environment of accident conditions, the oxidation rate of current Zr-based alloys rapidly increases. This results in hydrogen generation and explosions. In addition, the release of radionuclides into the environment is directly caused by the ballooning and opening of Zr-based alloy cladding during accident conditions. Thus, it is known that fuel claddings have to maintain their

* *Corresponding author.*
E-mail address: hgkim@kaeri.re.kr (H.-G. Kim).

http://dx.doi.org/10.1016/j.net.2015.11.011
1738-5733/

inherent performance during normal operation, as well as in accident conditions, to enhance the reliability and safety of nuclear power plants. From this, the development of accident-tolerant fuel (ATF) is a major concern of LWR research at present [2–8].

In comparison with the standard UO_2–Zr alloy system, ATF can tolerate loss of active cooling for a considerably longer period than current fuels, while maintaining or improving performance during normal operations and operational transients. It can also enhance fuel safety for beyond-design-basis events [1]. In detail, ATF includes design and/or material characteristics that prevent or delay the release of radionuclides during an accident event. The accident-tolerant characteristics may also include improvements in the integrity of fission product (FP) barriers [9]. ATF concepts basically consist of two components: fuel pellets and fuel cladding.

Several ATF pellet concepts are currently being suggested and evaluated around the world to mitigate the consequences of an accident [1,10–14]. Desirable attributes for ATF pellets include enhancing the thermal conductivity and retention of FPs. A high uranium density fuel is also desired, in particular, ATF cladding concepts, to compensate for the anticipated reduction of the fuel cycle length [15,16]. For example, a ceramic composite cladding likely gives rise to a smaller volume of fuel pellets owing to the thick cladding wall and low thermal conductivity [15,16]. Advanced non-Zr-alloy claddings, meanwhile, have a high neutron absorption cross section [7]. To alleviate the cost penalty, therefore, it might be necessary to use high-density pellets in combination with the proposed ATF cladding materials.

Many ATF cladding concepts are being considered to improve on the performance of current Zr-based alloys, especially in terms of oxidation resistance and mechanical strength under accident conditions [2–8]. The research concepts for enhanced ATF cladding development consist of Mo–Zr cladding [3], cladding coating [4,5], iron-based alloy cladding [7,8], and SiC_f/SiC cladding [8]. Regarding the ATF designs, cladding concepts must consider various factors such as safety, economics, fuel cycle, technological challenge, and the development schedule. As a midterm application, coating, iron-based alloy, and Mo–Zr claddings are being developed, whereas silicon carbide (SiC) cladding is considered a long-term application.

At the Korea Atomic Energy Research Institute (KAERI), two kinds of ATF pellet concepts are being evaluated [1,17–19]. As for midterm technology, a microcell UO_2 pellet is being studied to enhance the retention capability of highly radioactive and corrosive FPs. Our focus is to use existing infrastructure, experience, and expertise to the maximum extent possible, so that this evolutionary concept can be used in the relatively near future. For the long-term perspective, we are studying nitride- and silicide-based composite pellets that have a high uranium density and high thermal conductivity. In addition, surface-modified Zr alloy and the SiC composite concepts are considered as an ATF cladding as a way to decrease hydrogen generation as well as to decrease the ballooning and rupture opening during accident conditions. The development plan of the surface-modified Zr alloy concept is focused on as a near-term application and that of the SiC composite concept is considered a long-term application. This article deals with the development status of ATF pellets and claddings for LWRs in Korea.

2. Development status of ATF pellet

2.1. *Microcell UO_2 pellets*

2.1.1. *Concepts and design*

Microcell UO_2 pellets are envisaged as having the potential to enhance the performance and safety of current LWR fuels under normal operation conditions as well as during transients/accidents. Fig. 1 shows the conceptual schematic of a microcell UO_2 pellet, where all UO_2 grains or granules are covered by thin cell walls. The cell walls are designed to provide multiple chemical traps or a physical barrier against the movement of volatile FPs, or to enhance the thermal conductivity of pellets. There are two kinds of microcell UO_2 pellets under development at KAERI, classified according to the material type composing the cell wall. The first is a metallic microcell UO_2 pellet and the second is a ceramic microcell UO_2 pellet.

The metallic microcell UO_2 pellet is a high thermal conductive pellet with a continuously connected metallic wall. Recent impact assessments of the thermal conductivity of the fuel in a loss-of-coolant accident (LOCA) progressing in a pressurized water reactor (PWR) showed that an increase in thermal conductivity reduces both the peak cladding temperature and the quench time of the fuel rod [20,21]. Mo and Cr were primarily selected as the wall materials for the metallic

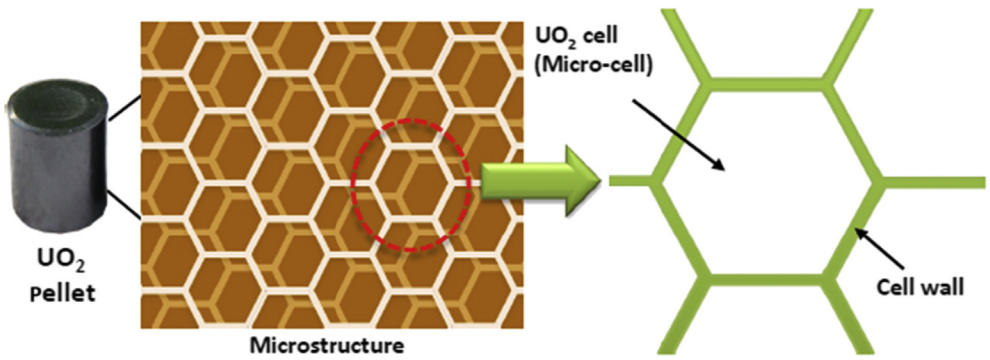

Fig. 1 – Conceptual schematic of microcell UO_2 pellet.

cell because they have relatively high melting temperatures, high thermal conductivity, and manageable neutron absorption cross sections.

The main purpose of the ceramic microcell UO_2 pellet is to minimize the FPs release contained in the pellet structure by providing a microcell structure with oxide additives [1]. An improvement in FP retention capability leads to a reduction of the inner surface cladding corrosion caused by FPs as well as the internal pressure of the fuel rod. A soft thin wall facilitates the fast creep deformation of the pellets, thereby reducing the mechanical loading of the cladding under operational transients. A mesh-like rigid wall structure is also expected to prevent the massive fragmentation of pellets during a severe accident.

Since the fission yield of cesium is roughly 10 times larger than that of iodine [22], the chemical affinity of the wall to cesium may have a deep impact on the retention capability of FPs. The recent ramp test result for additive-doped UO_2 pellets demonstrated that the additive phases for both Al–Cr and Al–Si contain increased amounts of Cs in the hot region of the pellets [23]. It was also shown that the Al–Si phase is better at retaining volatile elements, including iodine, within the fuel. This result suggests the chemical trapping of volatile FPs in an additive phase and a decreased possibility of the availability of aggressive species in the inside cladding. Based on the thermodynamic calculation results, we selected several SiO_2-based mixed oxides as additive candidates for ceramic cell wall materials.

2.1.2. *Fabrication and performance feasibility*

Fig. 2 respectively shows the shape and typical microstructure of 5 vol.% of Mo and 5 vol.% of Cr phase containing metallic microcell UO_2 pellets, in which the microcell concept is successfully implemented. These pellets were fabricated by the cosintering of metal powder coated UO_2 granules through a conventional sintering process. A detailed examination of the pellet microstructure suggests that a sound pellet without cracks is formed when the wall thickness remains around 5 μm [18].

Fig. 3A shows the thermal conductivity measurement results for the metallic microcell UO_2 pellets. Compared to standard UO_2 pellet, thermal conductivity was remarkably increased in the metallic microcell UO_2 pellets. Computer simulation has been applied to assess the effect of cell geometry on the thermal conductivity [24]. When the cell size and wall volume are fixed, the thermal conductivity more effectively increased when the cell elongates along the direction of thermal propagation. This prediction agrees well with the experimental results as shown in Fig. 3B. By contrast, the variation of cell size has little effect on the thermal conductivity if the wall volume and aspect ratio are fixed.

Several out-of-pile tests have been performed to preliminarily evaluate the fuel behaviors under normal operating conditions as well as in accident conditions [25,26]. Both standard UO_2 and metallic microcell pellets maintained their initial shape and microstructure after a LOCA simulating rapid heating test, in which the samples were heated from room temperature (RT) to 1,200°C with a heating rate of 20 K/s. A thermal transient annealing test showed that structural integrity for both Cr and Mo containing metallic microcell pellets were preserved well, even after the pellets were annealed at higher temperature than the melting point of the wall.

Pellet behavior under a high temperature steam environment needs to be evaluated because when the fuel rod is breached, high-temperature coolant penetrating through the defect [27] may react with the Cr or Mo wall to form oxide phases [28]. The preliminary steam oxidation test at 500°C showed that the metallic microcell UO_2 pellets retained their structural integrity much longer compared with the standard UO_2 pellets. By contrast, a steam oxidation test at 1,100°C revealed that the Mo wall vanished owing to a formation and evaporation of the volatile oxide phase. In the case of pellets containing Cr, the formation of the Cr_2O_3 phase, of a low density, resulted in the swelling and cracking of the pellets. We are now modifying the wall material by alloying with Al or Si. Formation of alumina or silica layers is expected to block, or at least retard, the growth of oxide layer growth in metallic walls.

The fabrication feasibility of ceramic microcell UO_2 pellets has been demonstrated [1,25]. The conventional liquid phase sintering technique has been applied. Fig. 4 shows the typical

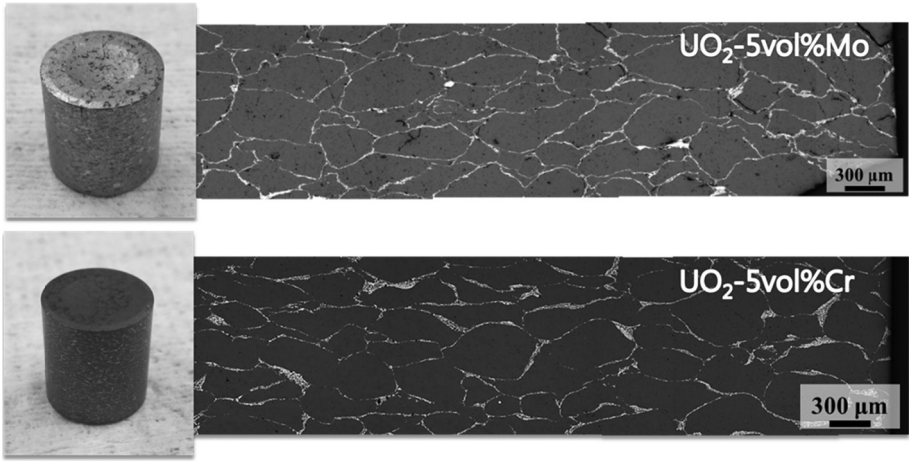

Fig. 2 – Sintered pellet shapes and relevant optical microstructures for 4.70 wt.% of Mo and 3.34 wt.% of Cr containing metallic microcell UO_2 pellets.

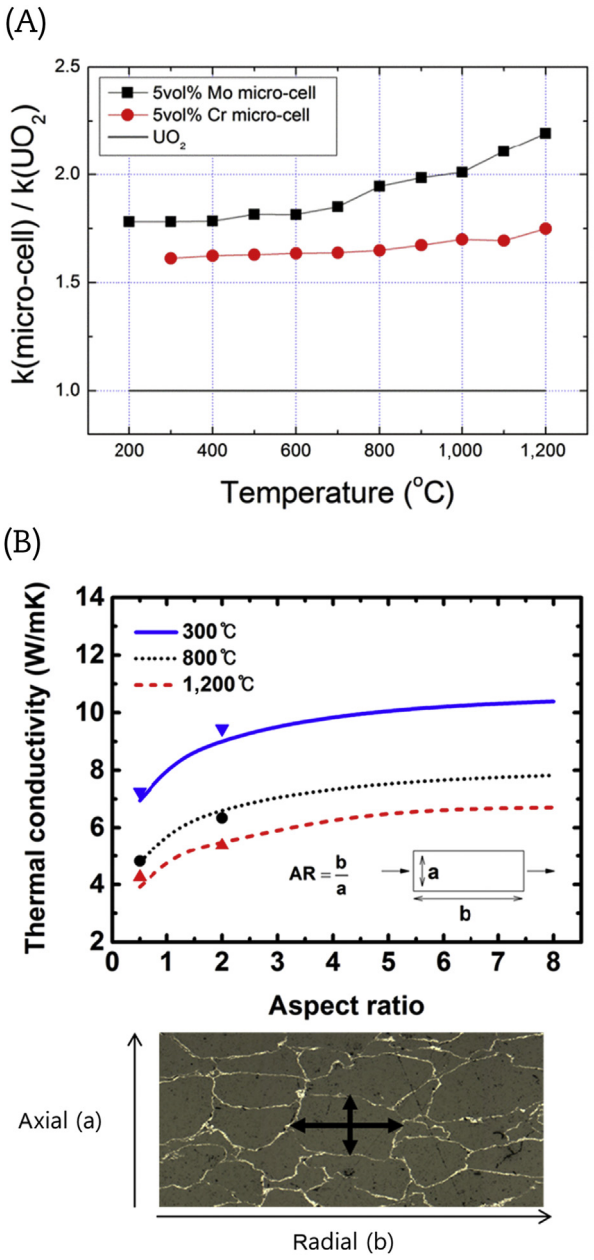

Fig. 3 – Thermal conductivity in metallic microcell UO_2 pellets. (A) Enhancement of thermal conductivity in metallic microcell UO_2 pellets, compared to standard UO_2. (B) Effect of cell geometry on the effective thermal conductivity of metallic microcell UO2 pellets. The lines are obtained by computer simulation and the dots are measured values.

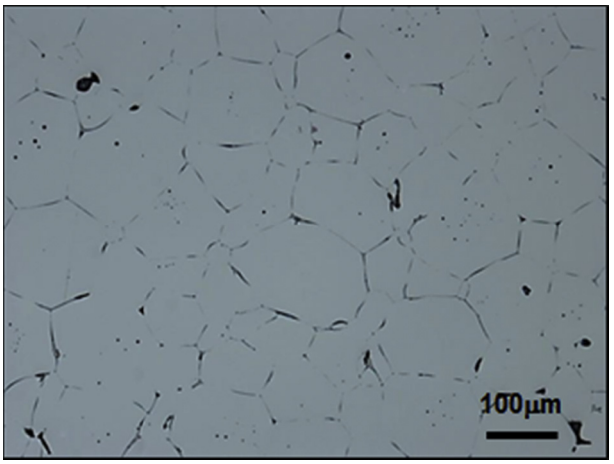

Fig. 4 – Optical microstructure of SiO_2–TiO_2 containing ceramic microcell UO_2 pellet.

microstructure of the ceramic microcell UO_2 pellet. This pellet was obtained by mixing 0.6 wt.% of SiO_2–TiO_2 oxides mixture with ADU-UO_2 powder and then sintering the powder mixture at 1,720°C for 4 hours in a dry hydrogen atmosphere. The sintered pellet density and average grain size for these pellets were 10.73 g/cm^3 and 80 μm, respectively.

The main benefit of ceramic microcell UO_2 pellets is an enhanced retention capability of the volatile FPs, such as Cs. A simple annealing test revealed the possibility that the Cs elements are preferentially segregated in the ceramic wall [1,25]. Thermal diffusivity and thermal expansion test results showed that the thermal properties of ceramic microcell UO_2 pellets are similar to those of a standard UO_2 pellet. By contrast, the compressive-creep deformation of ceramic microcell pellets at high temperature was faster than that of a standard UO_2 pellet. Fast creep deformation implies that the ceramic microcell pellets can reduce the cladding strain during a transient or accident, as well as during normal operation.

In contrast with the metallic wall, the ceramic wall is an oxide phase with inherent stability under a steam environment. Experimental results showed the enhanced resistance to steam oxidation in a ceramic microcell UO_2 pellet. A LOCA simulating rapid heating test and a thermal transient test at a higher temperature than the melting point of ceramic wall also revealed that the structural integrity of pellets was well preserved after the test.

Neutronics calculations were performed to preliminarily evaluate the impact of microcell UO_2 pellet concepts on fuel cycle length and economy [29]. The fuel assembly considered in the analysis was a 16 × 16 PWR fuel for OPR-1000. The reference fuel rod consists of 4.6 wt.% of U^{235}-enriched UO_2 pellets and Zircaloy-4 clad for a 3 × 18-month fuel management. Table 1 shows the calculation results. The effective full power day for the reference rod is 482. Because of the high neutron absorption of Cr and Mo, the cycle lengths for both metallic microcell fuel rods are much reduced in metallic microcell pellets. Consequently, the required amount of U^{235} in a metallic microcell UO_2 pellet to manage the 3 × 18-month fuel cycle is higher than that of reference UO_2, as shown in Table 1. The reduction of fuel cycle length or enrichment of U^{235} will increase the fuel cycle cost. When we only consider the enrichment cost [30], a fuel fabrication cost for a 4.70 wt.% of Mo and 5.55 wt.% of U^{235} containing metallic microcell UO_2 loaded fuel, was estimated to be about 17% higher than that for a reference UO_2 fuel. The Mo^{95} isotope (~15.9% in molybdenum) is mostly responsible for the neutron absorption in molybdenum. Therefore, using molybdenum depleted in Mo^{95} would mitigate the impact on the uranium enrichment. In the case of ceramic microcell UO_2 pellets, the impact on fuel cycle

Table 1 – Comparison of the fuel cycle length for reference UO_2 and microcell UO_2 fuels.

Case	Ref.	1	2	1	2	1	2
Fuel pellet	UO_2	UO_2 + Cr (3.34 wt.%, 5 vol.%)		UO_2 + Mo (4.70 wt.%, 5 vol.%)		UO_2 + SiO_2·TiO_2 (0.6 wt.%, ~2 vol.%)	
U enrichment (wt.%) (Normal)	4.60	4.60	5.15	4.60	5.55	4.60	4.65
U enrichment (wt.%) (Zoned)	4.10	4.10	4.65	4.10	5.05	4.10	4.15
Initial HM (g/m^3)	1,143.0	1,085.7	1,085.7	1,085.7	1,085.7	1,120.4	1,120.4
Cycle length (EFPD)	482.5	433.4	481.3	387.6	483.3	475	481

EFPD, effective full power day; HM, heavy metal.

was found to be negligible because the wall volume is smaller than that in metallic microcell pellets, and the neutron absorption due to Si is very small.

2.2. *High uranium density pellets*

The exploration of UO_2–uranium mononitride (UN) and UO_2–uranium silicide (U_3Si_2) composite fuels is ongoing for a long-term application. UN and U_3Si_2 are known to have many benefits, such as higher uranium density and thermal conductivity [19,31–34]. However, there are several drawbacks in the utilization of UN or U_3Si_2 as a fuel for water reactors. In this study, the feasibility of composite fuel concepts in which the uranium nitride or uranium silicide particles are embedded in a UO_2 matrix is being evaluated. These concepts are based on the assumption that a protective matrix of UO_2 would prohibit water corrosion of the nitride phase [19,35] or suppress irradiation swelling or chemical interaction of silicide at temperatures relevant to LWR operation [33].

Fabrication feasibility of dense pellets of UO_2–UN composite has been demonstrated by a hot pressing technique [19]. A phase analysis indicated that the sintered composites have a distinct feature in that the UN particles are surrounded by a UO_2 matrix, suggesting that the oxidation of UN particles in a composite fuel might be retarded because of the protection layer of UO_2. The density and thermal conductivity measurement results show that UO_2–UN composite fuels offer benefits of high uranium loading and enhanced thermal conductivity compared to current UO_2 nuclear fuels. Assessment of the oxidation reaction with coolant water and steam for the fabricated composite pellets is ongoing. If necessary, the composite pellet design will be modified to improve the waterproofness. Optimizing the microstructure, adding alloying elements, and providing an additional protective layer could be possible considerations.

Spherical U_3Si_2 powder from centrifugal atomization [36] was comminuted in a high-energy planetary mill to obtain fine powder. The resulting powder was sintered to a pellet under flowing Ar gas at a temperature of 1,773 K to preliminarily identify the phase components existing in a comminuted powder. X-ray diffraction and energy-dispersive spectrometry (EDS) examination of the uranium silicide pellets shows the majority of the pellets are U_3Si_2 with minor phases of silicon-rich uranium silicide and UO_2. The mixed powder of UO_2 and uranium silicide will be sintered to composite pellets to study the feasibility of utilization in current LWRs and advanced power reactors as well.

2.3. *In-reactor irradiation test plan*

An irradiation program for microcell UO_2 pellets under bilateral cooperation with the International Thorium Consortium is ongoing. The main objective is to study the thermomechanical and fission gas release (FGR) behavior of microcell UO_2 pellets, by irradiating highly instrumented fuel rods under normal PWR operating conditions in the Halden reactor. Table 2 shows the specification of pellets for the Halden irradiation test. The focus is on the fuel performance parameters such as fuel centerline temperature, fuel densification and swelling, and FGR behavior. After the irradiation test, several postirradiation tests will be performed to evaluate the fission damage on the wall structure, transport kinetics of volatile FPs through or along the wall to the cladding inside, chemical interactions between the wall and FPs, and redistribution of wall components in a pellet, and so on.

3. Development status of ATF cladding

3.1. *Surface-modified fuel cladding*

3.1.1. *Concepts and design*

The major benefit of the surface-modified fuel cladding concept is the economics because the commercial Zr-based alloy and manufacturing facility can be continuously

Table 2 – Specification of microcell fuel pellets irradiating in Halden reactor.

Cell wall materials	Ceramic microcell UO_2	Metallic microcell UO_2
	0.6 wt.% Si–Ti–O (2 vol.%)	3.4 wt.% Cr (5 vol.%)
Averaged cell size (μm)	~80	~290
Pellet density (g/cm^3)	10.73 ± 0.03	10.45 ± 0.03
Pellet diameter (mm)	8.190 ± 0.002	8.196 ± 0.001
Pellet height (mm)	9.4 ± 0.2	9.12 ± 0.03
Pellet weight (g)	5.15 ± 0.10	4.93 ± 0.02
U^{235} enrichment	4.5%	4.5%

operated by developing the surface-modified cladding concept. In addition, the surface modification on Zr-based alloy cladding has a high melting point, high neutron economy, and high tritium permeation when compared to iron-based alloy cladding. However, the challenge of the surface modification by coating Zr-based alloys is the lower mechanical strength at higher temperatures than the iron-based alloy, and the resolution of the adhesion properties of Zr-based alloy and the coating materials. It was reported that the major challenges for surface modification by coating include the careful matching of the thermal expansion coefficient, which is related to the delamination of the coated layer during the thermal cycles [36]. Moreover, the surface modification by coating must be compliant enough to withstand the diametrical variation regarding the creep deformation of cladding, and to withstand the change in axial length regarding the irradiation growth of Zr alloy cladding [36]. From this, the interface property between Zr-based alloy and the coating materials is one of the important technical issues in the application of fuel cladding. Because the high temperature strength of the surface modification by coating cannot be improved when compared to the commercial Zr-based alloy, partial oxide dispersion strengthened (ODS) treatment as a surface modification technology is thought to increase the cladding strength, which is related to the ballooning and rupture behavior of cladding during accident conditions [37]. By a combination of two types of surface modification technology of the surface coating and partial ODS treatment, the oxidation resistance and strength at high temperature can be considerably improved over Zr-based alloy cladding. Thus, we concluded that the surface modification technology showed promise for application to ATF cladding as a near-term application concept.

3.1.2. *Development of surface modification by coating technology*

Various coating technologies, such as a plasma spray, chemical/physical vapor deposition, and laser cladding, have been applied in the commercial industry to control the surface properties of components. Among them, we considered laser coating as a direct application method on the fuel assembly components with a complex shape (cladding tube, guide tube, and spacer grid). A coating method with a high vacuum control is not preferable from an economic point of view because the length of the cladding and guide tube is 4 m, and the temperature during the coating process cannot be increased by more than the final annealing temperature of Zr-based alloy cladding (about 500°C in general) to avoid a microstructural change, because the cladding properties are affected by the annealing temperature. In addition, the coating process can be applied to an irregular surface shape, because the coated components in the fuel assembly have an irregular shape (tubular and deformed plate grid). For these reasons, the three-dimensional (3D) laser coating technology supplied with powder was selected to apply the coating of the fuel assembly components [5]. To develop the 3D laser coating technology, we systematically studied the laser beam power, inert gas flow, cooling of the cladding tube, and powder control as key points for obtaining the soundness of the coated layer. After Cr coating on the Zr-based cladding, ring compression and ring tensile tests were performed to evaluate the adhesion properties between the coated layer and the Zr-based alloy tube at RT, and a high-temperature oxidation test of the coated tube samples was conducted to evaluate the oxidation behavior at 1,200°C.

Fig. 5 shows the appearance of the 3D laser coating process and cross-sectional scanning electron microscopy (SEM) observation of the Cr-coated layer [38]. Through coating parameter optimization, the Cr-coated layer with a length of 100 mm can be made on a Zircaloy-4 cladding tube surface without crack formation, surface oxidation, or deformation of the axial or hoop direction of the cladding tube. The coated area showed a rough surface, because the melted Cr particles were attached on the coated surface during the coating process as shown in Fig. 5 in the middle part. However, this rough surface can be easily controlled by a grinding process using SiC paper. From the cross-sectional observation using SEM, as shown in Fig. 5, it was revealed that the Cr layer was well attached to the Zircaloy-4 cladding surface, and the mean thickness of the coated layer was about 80 μm.

Fig. 6 shows the engineering stress and the strain curves of the ring tensile test in the left part and ring compression test in the right part of this figure, as well as the sample appearance after the tests [38]. The thickness of the Cr-coated layer of 80 μm, which was identified in the cross-sectional SEM observation in Fig. 5, was calculated in both ring tests. The variation trend of stress–strain curves was similar between the reference and Cr-coated cladding, although the strength of the Cr-coated samples was somewhat increased when compared with that of the reference samples in both the tensile and compression tests. Peeling or spalling phenomena were not observed in the tested samples, although the Cr-coated layer was cracked at the severe deformed region after both tests. Regarding the crack formation of Cr-coated cladding tube during the hoop direction deformation, the detailed strain value for making a crack has to be checked to determine the coated layer quality. A ring tensile test with strain variations of 2%, 4%, and 6% was performed for the Cr-coated cladding tube using 3D laser coating. After the ring tensile test reached each target strain of 2%, 4%, and 6%, the cross-sectional observation using SEM was performed to evaluate the microstructural behavior. The Cr-coated layer showed a no-defect microstructure of up to 4% strain, whereas the lateral cracks were formed in the Cr-coated layer after 6% strain. In addition, the interface between the Cr-coated layer and Zircaloy-4 matrix was maintained without peeling, although the Cr-coated layer was cracked by the 6% strain. From this, it was determined that the crack initiation of Cr-coated cladding using 3D layer technology was clearly suppressed up to a 4% strain, which satisfies the 1% strain of the fuel cladding specifications.

Fig. 7 shows the cross-sectional SEM observation of the Cr-coated Zircaloy-4 cladding using 3D laser coating technology and the reference Zircaloy-4 cladding after the high-temperature oxidation test at 1,200°C for 2,000 seconds in a steam environment [38]. The oxidation behavior was determined using an SEM image and EDS analysis results. It was clearly shown that the Cr-coated layer on the Zircaloy-4 tube was maintained without spallation or severe oxidation, and the thickness of the oxide layer was less than 4 μm. However,

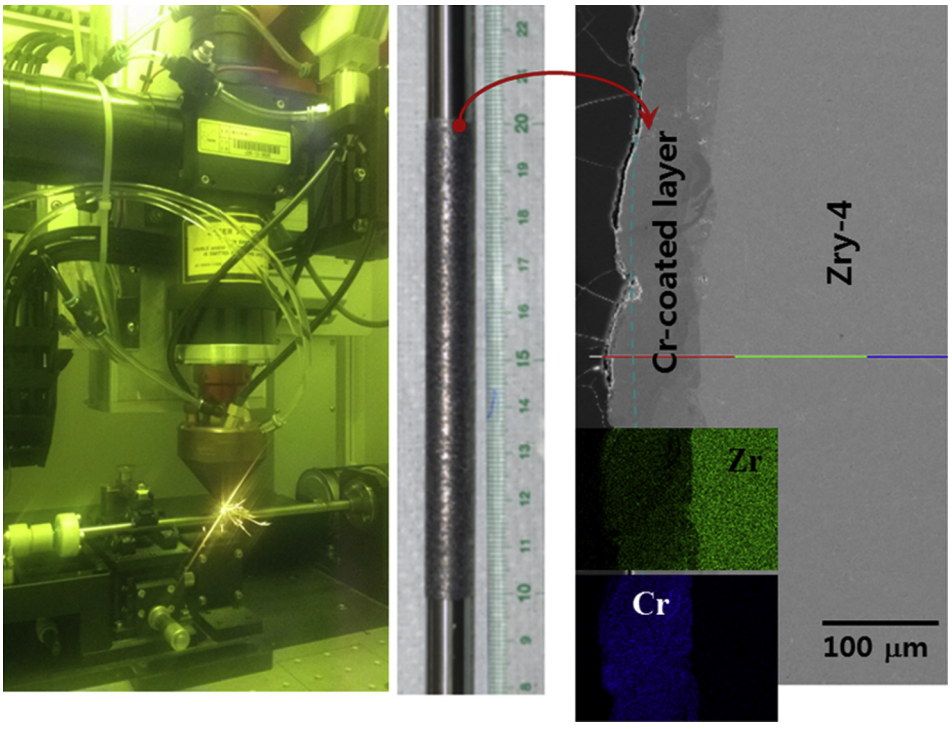

Fig. 5 – 3D laser coating process supplying the Cr powder, surface appearance, and cross-sectional analysis of the Cr-coated Zircaloy-4 cladding tube [38].

the thickness of the ZrO_2 layer formed on the uncoated Zircaloy-4 cladding tube surface was about 113 μm. It was expected that the oxygen diffusion through the Cr-coated layer would be effectively prevented during the high-temperature oxidation test, since the α-Zr(O) phase layer was not formed at the interface between the Zircaloy-4 matrix and Cr-coated layer, as shown in the SEM micrograph.

From the out-of-pile study on the surface-modified Zr cladding by coating technology, it was revealed that the Cr-coated layer was not peeled off after the ring tensile and

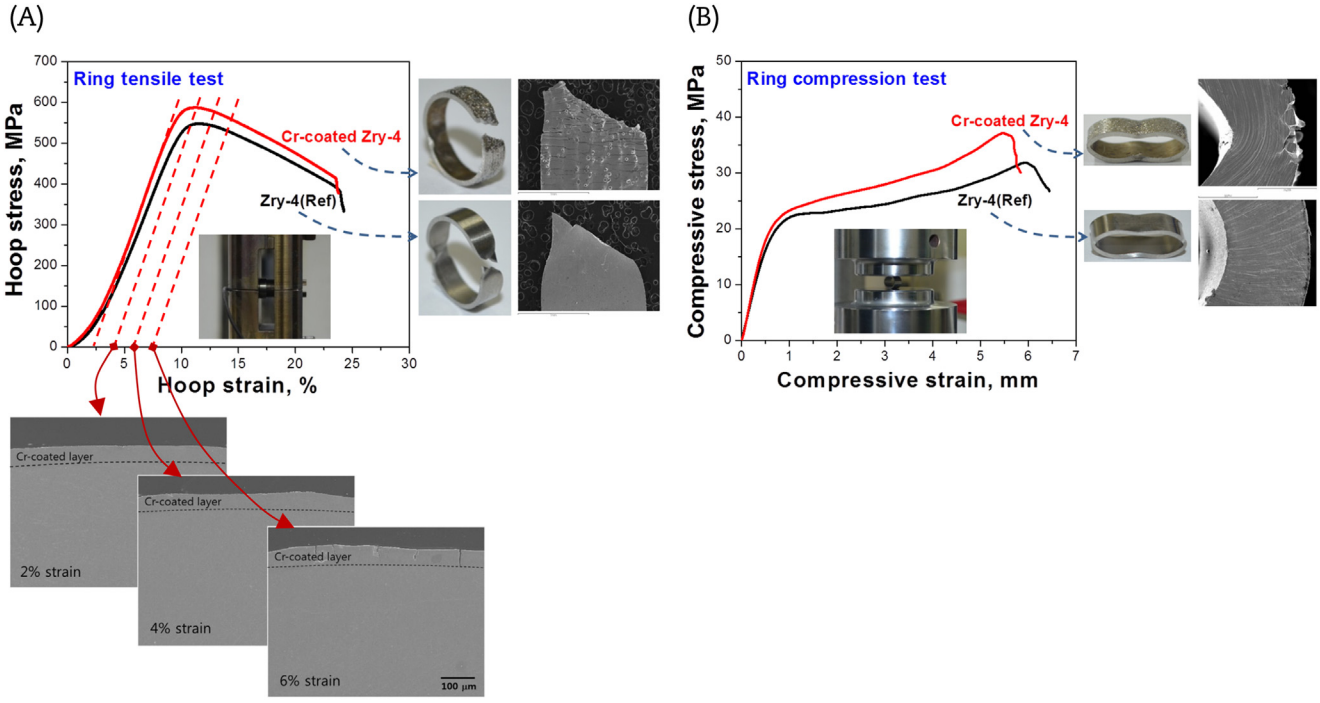

Fig. 6 – Ring tensile test result and sample appearance of the Cr-coated Zircaloy-4 cladding tube (A), and ring compression test result and sample appearance the Cr-coated Zircaloy-4 cladding tube (B) [38].

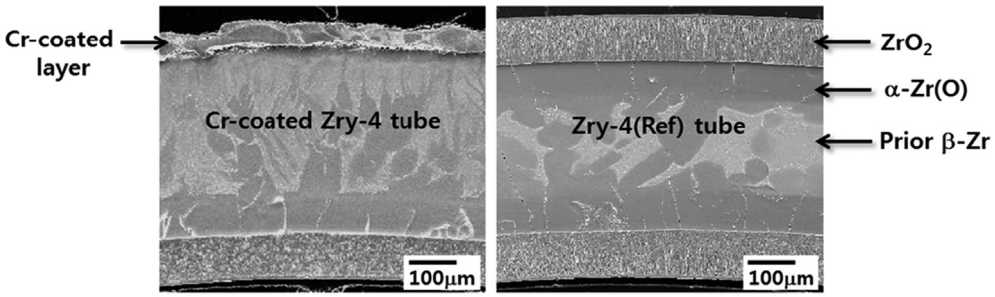

Oxide thickness	
Cr-coating	Zry-4
4 μm (1/30 of Zry-4)	113 μm

Fig. 7 – Cross-sectional scanning electron microscopy observation of the Cr-coated Zircaloy-4 cladding using 3D laser coating and the reference Zircaloy-4 cladding after the high-temperature oxidation test at 1,200 °C for 2,000 seconds in a steam environment [38].

compression tests, although some cracks were formed on the Cr-coated layer by a hoop direction deformation, which was higher than 4%. The oxide thickness formed on the Cr-coated layer was about 30 times thinner than that formed on a Zircaloy-4 tube surface.

3.1.3. *Development of surface modification by partial ODS technology*

The partial ODS technology is developed to increase the strength of the zirconium-based alloy up to high temperatures. The detailed procedure used to make an ODS layer on the Zircaloy-4 surface was described in a previous study [37]. Fig. 8 shows the surface appearance after laser beam scanning (LBS) of the Y_2O_3 powder spread on a Zircaloy-4 sheet, and cross-sectional optical microscopy (OM) and SEM observations of the ODS-treated region. In the OM observation, the melted zone with a 0.4-mm layer thickness was shown as having a fine grain structure, and a heat-affected zone with a 0.3-mm layer thickness was observed between the melted zone and the recrystallized grain region (initial substrate structure of the Zircaloy-4 sheet). The melted zone was very quickly cooled after the laser beam scan, and therefore, the zone was transformed into a martensite structure. From the cross-sectional observation by SEM, it was identified that a wave shape was formed at the substrate and ODS-treated layer interface. This wave interface was caused by a repeated LBS line with a beam diameter of about 130 μm on the Zircaloy-4 surface, which could be seen in the surface observation. The thickness of an average ODS-treated layer of the Zircaloy-4 sheet was about 0.4 mm, and this thickness reached about 20% of the initial Zircaloy-4 sheet thickness. In a high-magnification SEM image, it was observed that the Y_2O_3 particles, which were identified by an SEM-EDS point analysis, were uniformly distributed in the reaction area. From this, the homogeneous mixing area between the Zircaloy-4 alloy matrix and Y_2O_3 particles can be obtained in

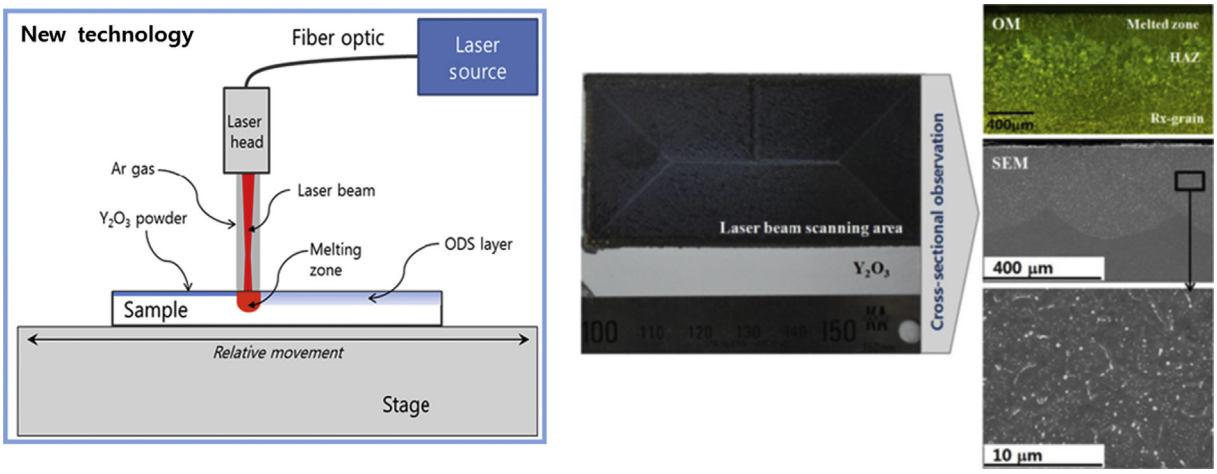

Fig. 8 – Surface appearance after laser beam scanning (LBS) on Zircaloy-4 sheet and cross-sectional observation of oxide dispersion strengthened alloying region [37]. ODS, oxide dispersion strengthened; OM, optical microscopy; SEM, scanning electron microscopy.

the melting zone. In addition, no voids or cracks in the ODS treated region were observed in this area [37].

Fig. 9 shows the engineering stress–strain curves of three types of prepared samples, consisting of the initial state Zircaloy-4 sheet (marked as initial sheet), surface laser beam scanned Zircaloy-4 sheet (marked as surface LBS), and surface laser beam scanned Zircaloy-4 sheet with Y_2O_3 oxide powders (marked as surface LBS with Y_2O_3 powder) [37]. The strength and ductility variations with the prepared samples were clearly shown at both RT and 500°C tests. In the RT test, the yield strength (YS) and ultimate tensile strength (UTS) were gradually increased by the surface LBS condition to the surface LBS with Y_2O_3 powder condition when compared to the initial state of the Zircaloy-4 sheet. However, the strain elongation behavior of the three tested samples was inversed when compared with the values of YS and UTS. In the 500°C test, the YS and UTS results were gradually increased by the surface LBS condition as well as the surface LBS with Y_2O_3 powder condition when compared to the initial state of the Zircaloy-4 sheet. In particular, the strength result was considerably improved by the surface LBS treatment with oxide powder. The uniform elongation region of three sample types in the 500°C test was very limited when compared to the RT test. In addition, the strain elongation of the LBS-treated surface and LBS-treated surface with oxide powder samples dropped sharply after the highest stress [37].

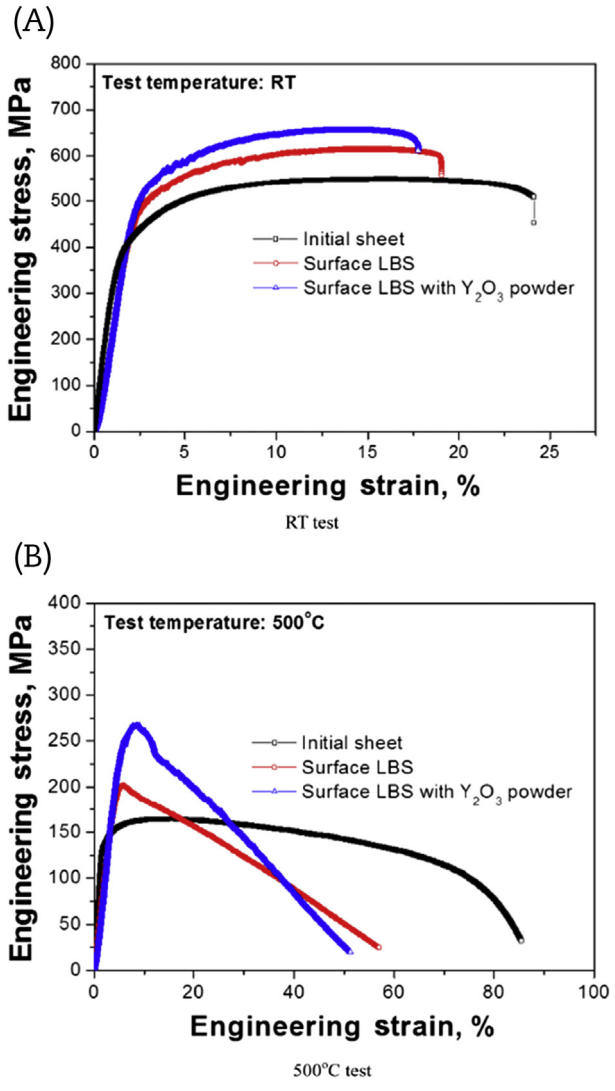

Fig. 9 – Engineering stress–strain curves of the different surface-treated Zircaloy-4 sheet samples. (A) Sample tested at room temperature. (B) Sample tested at 500°C [37]. LBS, laser beam scanning; RT, room temperature.

Regarding the partial ODS technology, the Y_2O_3 particles can be successfully dispersed in a Zircaloy-4 sheet surface using an LBS method. Submicron Y_2O_3 particles were uniformly distributed in an ODS alloyed layer using laser technology without voids or cracks. From the tensile test at 500°C, the strength of laser ODS alloying on the Zircaloy-4 sheet was increased more than 65% when compared to the initial state of the sheet, although the ODS alloyed layer was 20% of the specimen thickness.

3.1.4. *In-reactor irradiation test plan*

The surface modification cladding has to be evaluated for the irradiation performance since the most important factor of ATF cladding materials is the in-pile performance such as the corrosion, creep, growth, and microstructural characteristics at the interface between the coated layer and Zr alloy under normal operation conditions. In order to qualify the irradiation performance, an irradiation test for the surface-modified Zr cladding will be started at the end of 2015 under the bilateral cooperation with an international consortium.

3.2. *SiC composite fuel cladding*

SiC ceramics, especially in their composite form (SiC_f/SiC composites), have superior high-temperature properties, excellent irradiation resistance, inherent low activation and other superior physical/chemical properties [39]. Compared to the current Zr alloys, the SiC composites also offer a reduced neutron absorption cross section and an outstanding oxidation resistance to high-temperature steam [40,41]. The combination of these attractive features makes the SiC composites one of the leading candidates for accident-tolerant LWR fuel cladding and core structures [40,42]. Although the SiC composites are expected to provide outstanding safety features under severe accident conditions, there are several key issues that need to be addressed for the LWR application, such as the fabrication of thin-walled long tubes, the hermetic joining of end-cap seals, and capability of FP retention, corrosion under the normal operating conditions of an LWR [10,15,43]. In the following sections, we introduce our fabrication efforts and mechanical properties of SiC composite tubes. Corrosion test results of chemical vapor deposition (CVD) SiC ceramics are summarized as well.

3.2.1. *Fabrication of multiplex SiC composite tubes*

SiC composite tubes consisting of a monolith SiC inner layer, a SiC_f/SiC composite intermediate layer, and a monolith SiC outer layer were fabricated by the CVD or chemical vapor infiltration (CVI) process. Fig. 10 shows images of the triplex structured tubes in different scales. We applied different fiber winding patterns and found that the surface roughness could be controlled within several

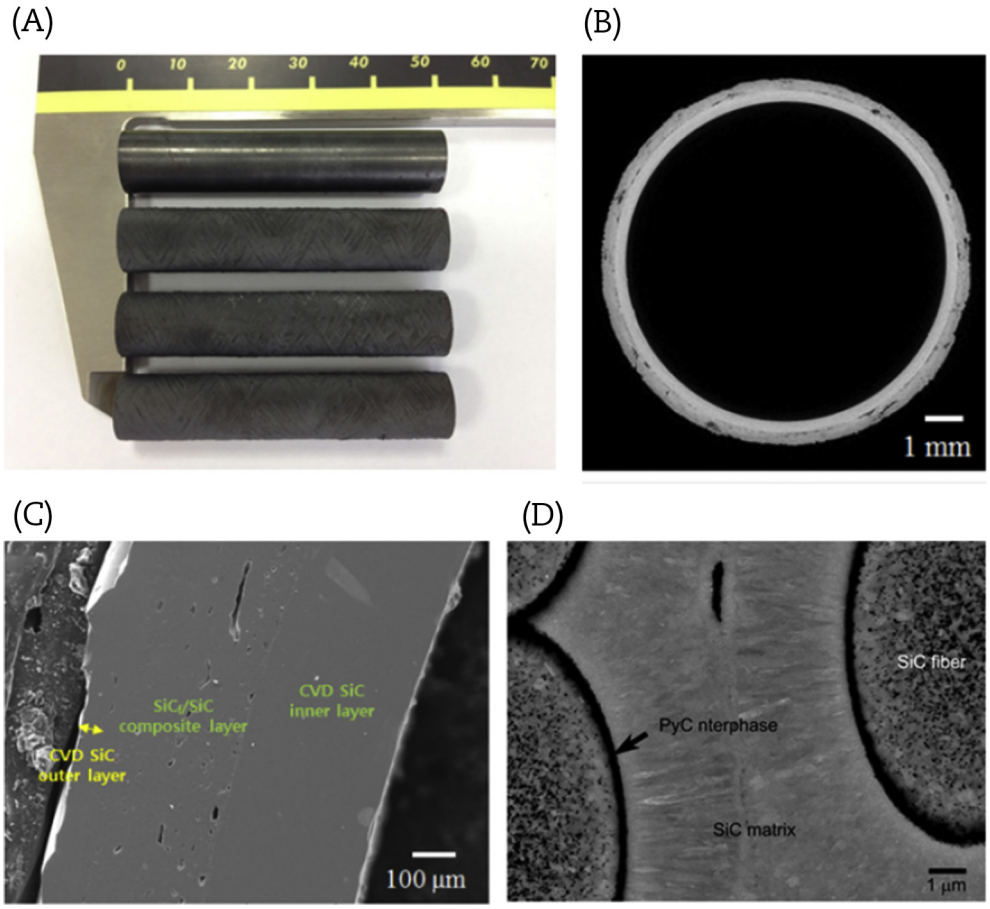

Fig. 10 – Images of triplex structured tubes in different scales. (A) Photograph of the triplex SiC composite tubes. (B) X-ray microcomputed tomography sliced image along the transaxial planes. (C) Scanning electron microscopy microstructure for the cross section. (C) Magnified view of the SiC$_f$/SiC composite layer.

micrometers after machining the outer surface (Fig. 10A). The monolith SiC inner layer was uniformly deposited with a thickness of 320.3 ± 6.4 μm, and the SiC$_f$/SiC composite layer had a similar thickness. The SiC outer layer was deposited with a thickness of about 50 μm (Fig. 10C). The SiCf/SiC composite layer consists of SiC fibers, pyrolytic carbon (PyC) interphase, and SiC matrix, as shown in Fig. 10D. The PyC interphase of about 200 nm in thickness was deposited onto the SiC fibers. The interbundle voids within the composite layer could be effectively densified by the CVI process with a composite density higher than 2.9 g/cm^3. Although some circumferential voids remained in the composite layer, the fraction of void was quite low compared to typical CVI-processed plain-woven SiC$_f$/SiC composites [44].

In order to examine the effects of fiber winding patterns and angles on the hoop strength of the triplex composite tubes, different winding patterns were applied by varying the fiber winding sequence. The SiC fibers used were Tyranno SA3 or Hi-Nicalon Type S fibers. As an example, Fig. 11 shows four phase winding patterns wound with the winding angle of ± 55° using Tyranno SA3 fiber. The winding pattern was controlled by adjusting the position of the second fiber trajectory. A detailed procedure and the effect of winding patterns on the fiber volume fraction and matrix densification behavior were described in our previous reports [44,45].

3.2.2. *Mechanical property of SiC composite tubes*

For the hoop test, a polyurethane plug was compressed inside a composite tube to evaluate its mechanical properties. Fig. 12 shows the ultimate hoop stresses of the SiC composite tubes as a function of the fiber volume fraction in the triplex tubes, and the type of reinforcement fiber. The fiber volume fraction of each tube is in the range of 18–25%. The hoop stress of the triplex tube tends to be proportional to the fiber volume fraction regardless of both the reinforcement fiber and fly number [44].

Fig. 13A displays a typical applied load versus the axial displacement curve of the composite tubes. The applied load gradually increases until the polymer plug contacts the inner wall of the tube at the initial stage, after which it increases steeply. It can also be observed that some load drops occur prior to the failure of the tube, which was caused by the formation of a crack in the inner monolithic SiC layer [44]. The fracture strengths of brittle materials such as SiC ceramics have a statistical distribution, described by the Weibull statistics [46]. Fig. 13B shows the Weibull plots for the ultimate hoop stress and the stress at the first load drop of SiC triplex composite tubes, measured

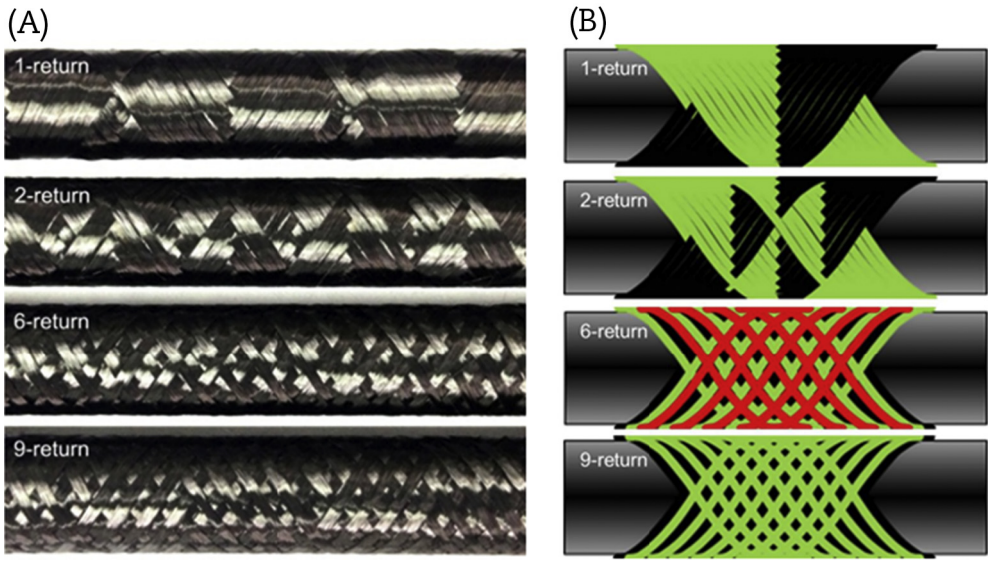

Fig. 11 – Winding patterns wound by a helical filament winding method using Tyranno SA3 fiber with the winding angle of ±55° [44,45]. (A) Four phase winding patterns. (B) Schematic illustrations.

for 20 tube samples. The average stress (σ_m) for ultimate failure is 282 MPa with the Weibull modulus of 11.05. By contrast, the average stress and Weibull modulus for the first load drop are 227 MPa and 5.30, respectively. The Weibull modulus for the hoop stress at the first load drop is much lower than that for the ultimate hoop stress. The initial load drop is associated with the onset of a significant axial crack in the monolithic SiC inner layer; and extensive matrix microcracks in the SiC_f/SiC composite layer also develop right after the failure of the SiC inner layer. This can lead to the release of FPs. As shown in Fig. 13B, if we assume the characteristic stress (σ_0) and Weibull modulus for the microcracking stress to be 245 MPa and 5.30, respectively, the applied stress on the composite cladding should be less than 20 MPa to maintain an FGR rate below 10^{-6}. Currently, we are trying different tube designs to increase the mechanical reliability of SiC composite tubes and the retention capability of FPs.

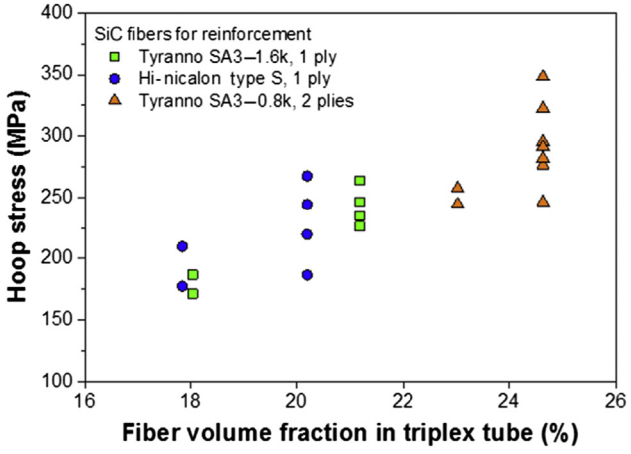

Fig. 12 – Hoop stresses of the SiC composite tubes as a function of the fiber volume fraction [44].

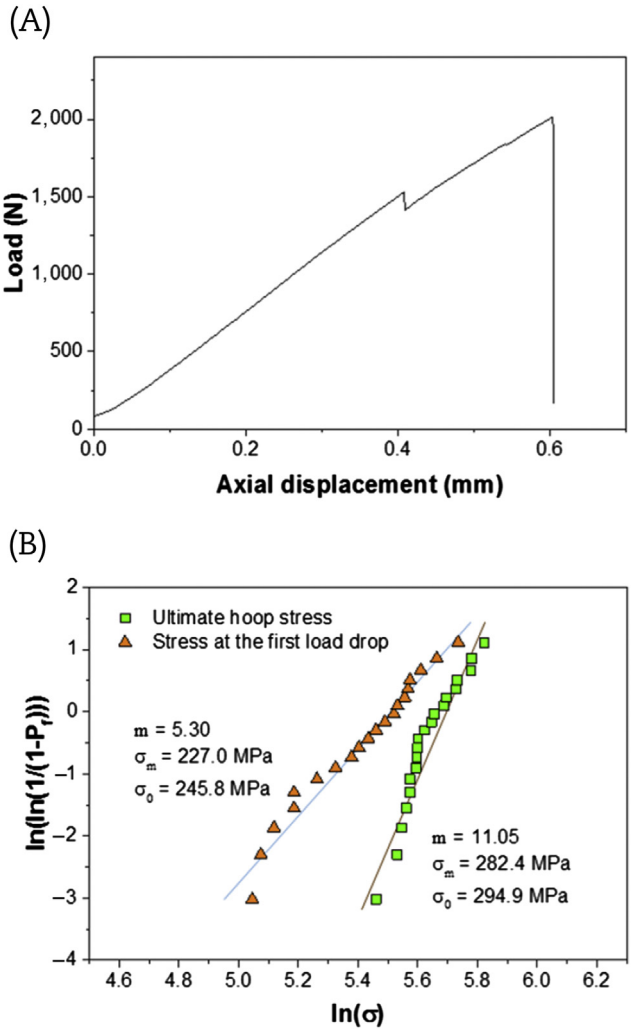

Fig. 13 – SiC composite tubes. (A) Typical load versus axial displacement curve. (B) Weibull plots for the ultimate hoop stress and the stress at the first load drop.

3.2.3. *Corrosion behavior of SiC in PWR-simulating water*

Several results have been reported with regard to the dissolution phenomena of SiC ceramics in hydrothermal water [47–50]. The dissolution phenomena of SiC in hydrothermal water reported in previous studies are problematic for the application of SiC to PWR fuel claddings. According to our previous results [47,49], the corrosion behavior of SiC is strongly affected by the dissolved oxygen content in water. The corrosion rate was much higher in the static autoclave containing several ppm of dissolved oxygen than in the loop test, in which the dissolved oxygen content was maintained at less than 5 ppb. However, there was also a considerable amount of corrosion even in the loop test when the dissolved hydrogen was not controlled. The grain boundaries of CVD SiC were preferentially attacked at the early stage of corrosion, and the grains became thinner. Some grains were detached from the surface, as shown in Fig. 14. We further evaluated the corrosion behavior of CVD SiC by controlling the dissolved hydrogen. Corrosion tests were carried out for up to 210 days using a simulated PWR water loop in which water was deoxygenated and pressurized at 360°C under 20 MPa. To simulate the PWR primary water chemistry, the dissolved oxygen and the dissolved hydrogen were maintained at below 5 ppb and at approximately 2.7 ppm (35 cc/kg H_2O), respectively. Deionized water was treated at pH 6.4 with 2.2 ppm LiOH and 1,200 ppm H_3BO_3.

Fig. 15 shows the weight change of CVD SiC specimens after corrosion tests at 360 °C in deoxygenated water with and without dissolved hydrogen. It can be seen that the weight loss significantly decreased in the PWR-simulating water loop test with dissolved hydrogen controlled. The corrosion rates calculated by the least square fit of the weight loss data were 9.4×10^{-5} and 3.5×10^{-2} mg/cm^2 day for the corrosion tests with and without the control of dissolved hydrogen, respectively. The corrosion rate decreased by about 400 times by the injection of hydrogen. Fig. 16 shows the SEM micrographs of the CVD SiC specimens prior to and after the corrosion tests in the simulated PWR water environment with the control of dissolved hydrogen. The surface microstructure hardly changed for up to 210 days after the corrosion tests. Compared with the previous corrosion test results [47–50], it is clear that the dissolution of SiC is extremely limited. Moreover, there was no evidence of a preferential corrosion at the grain boundaries or of a pitting corrosion. However, for an assessment of the corrosion resistance of SiC in the PWR coolant water, the effects of irradiation and microstructure variation of CVD SiC on the corrosion behavior of SiC need to be further evaluated.

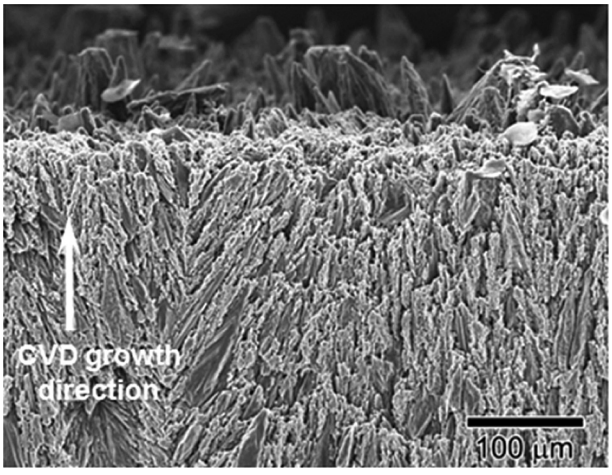

Fig. 14 – Scanning electron microscopy micrograph for the side surface of chemical vapor deposition SiC after corrosion test at 360 °C for 300 days in the pressurized water reactor-simulating water without controlling the dissolved hydrogen [51]. CVD, chemical vapor deposition.

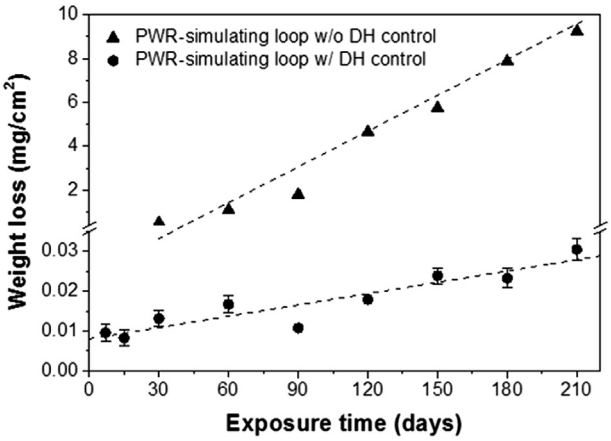

Fig. 15 – Corrosion behavior of chemical vapor deposition SiC specimens at 360°C in pressurized water reactor-simulating water loops with and without controlling the dissolved hydrogen [51]. PWR, pressurized water reactor.

4. Summary

In order to considerably improve the safety of LWRs under accident conditions, the innovative fuel pellet and claddings (ATF) are being proposed and developed at present. In Korea, the microcell UO_2 concept and high uranium density composite concept are considered as ATF pellets to capture the radioactivity in the pellet structure and to decrease the fuel temperature during accident conditions. In addition, the surface-modified Zr alloy and the SiC composite concepts are considered as an ATF cladding to decrease the hydrogen generation and to decrease the ballooning and rupture opening during the accident conditions. The ATF pellet and cladding concepts developed in Korea can be summarized as follows.

(1) Development of microcell UO_2 and high-density composite pellets

Fabrication feasibility for microcell UO_2 pellets and UO_2–UN composite pellet has been demonstrated. Thermophysical property measurements under normal operating and selected accident conditions showed that design concepts are successfully implemented in fabricated pellets. For microcell UO_2 concepts, the composition of the metallic wall is being modified to improve the chemical stability with high-

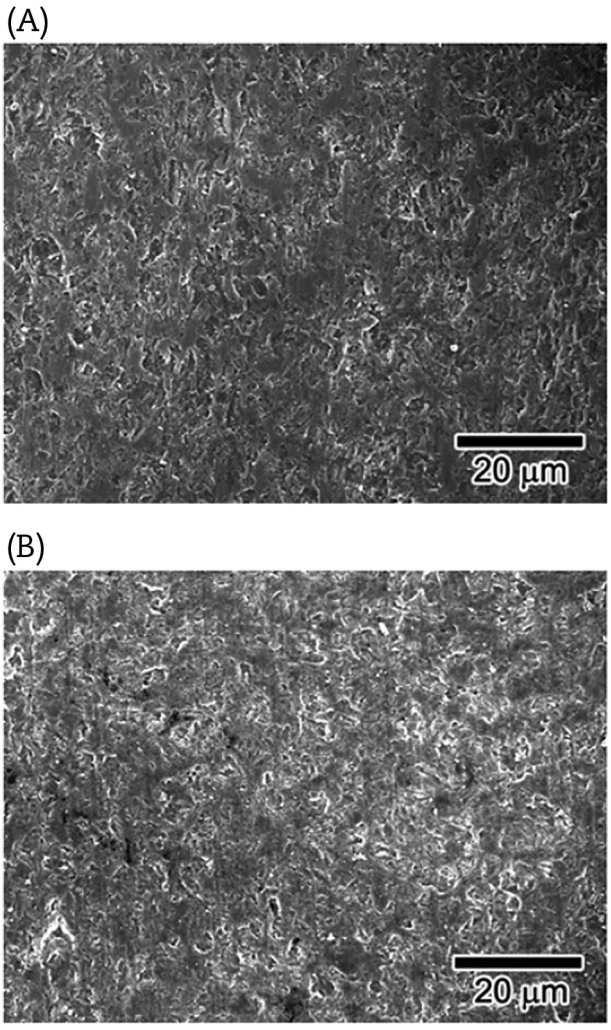

Fig. 16 – Scanning electron microscopy micrographs for the top surfaces of chemical vapor deposition SiC specimens. (A) Prior to corrosion test. (B) After corrosion test for 210 days in the pressurized water reactor-simulating water with controlling the dissolved hydrogen [51].

temperature steam. A primary challenge for high-density composite pellets is an optimization of pellet design that can enhance the waterproofness of pellets. The irradiation test with highly instrumented fuel rods under normal PWR operating conditions in the Halden reactor is also an important ongoing mission.

(2) Development of surface-modified fuel cladding

The surface modification cladding concept is promising as an ATF cladding. It may also be applied without major changes in the substrates of zirconium-based alloys, because this cladding concept has a good oxidation (corrosion) resistance, as well as an improved strength at high temperatures when compared with commercial Zr alloy claddings. An irradiation test on the surface-modified Zr cladding will be started in order to qualify the irradiation performance, such as corrosion, creep, irradiation growth, and adhesion properties.

(3) Development of SiC composite fuel cladding

The corrosion of SiC under PWR-simulating water conditions was significantly reduced with the control of dissolved hydrogen, by retarding the formation of the surface oxide layer. Fiber winding patterns affected the hoop strength of SiC composite tubes, mainly due to the difference in fiber volume fraction. Efforts on optimal tube designs are in progress for an improvement of mechanical reliability of composite tubes.

Conflicts of interest

All authors have no conflicts of interest to declare.

Acknowledgments

This work was supported by the National Research Foundation of Korea (NRF) grant, funded by the Korea government (MSIP) (NRF-2012M2A8A5025821, 2012M2A8A5025822, and 2015M2A8A4001841).

REFERENCES

[1] Y.H. Koo, J.H. Yang, J.Y. Park, K.S. Kim, H.G. Kim, D.J. Kim, Y.I. Jung, K.W. Song, KAERI's development of LWR accident-tolerant fuel, Nucl. Technol. 186 (2014) 295–304.
[2] J. Carmack, F. Goldner, S.M. Bragg-Sitton, L.L. Snead, Overview of the U.S. DOE accident tolerant fuel development program, TopFuel 2013, Charlotte, North Carolina, Sep. 15–19, 2013.
[3] B. Chang, Y.J. Kim, P. Chou, J. Deshon, Development of Mo-alloy for LWR fuel cladding to enhance fuel tolerance to severe accidents, TopFuel 2013, Charlotte, NC, Sep. 15–19, 2013.
[4] I. Idarraga-Trujillo, M. Le Flem, J-C. Brachet, M. Le Saux, D. Hamon, S. Muller, V. Vandenberghe, M. Tupin, E. Papin, E. Monsifrot, A. Billard, F. Schuster, Assessment at CEA of coated nuclear fuel cladding for LWRs with increased margins in LOCA and beyond LOCA conditions, TopFuel 2013, Charlotte, NC, Sep. 15–19, 2013.
[5] H.G. Kim, I.H. Kim, J.Y. Park, Y.H. Koo, Application of Coating Technology on Zr-based Alloy to Decrease High-temperature Oxidation, Zirconium in the Nuclear Industry STP 1543, 2013, http://dx.doi.org/10.1520/STP154320120161.
[6] B.A. Pint, K.A. Terrani, M.P. Brady, T. Cheng, J.R. Keiser, High temperature oxidation of fuel cladding candidate materials in steam-hydrogen environments, J. Nucl. Mater. 440 (2013) 420–427.
[7] K.A. Terrani, S.J. Zinkel, L.L. Snead, Advanced oxidation-resistance iron-based alloys for LWR fuel cladding, J. Nucl. Mater. 448 (2013) 420–435.
[8] J.D. Stempien, D.M. Carpenter, G. Kohse, M.S. Kazimi, Characteristics of composite silicon carbide fuel cladding after irradiation under simulated PWR conditions, Nucl. Technol. 183 (2013) 13–29.
[9] R. Montgomery, E. Mader, N. Domenico, R. Fawcett, J. Guerci, E. Lahoda, B. Minnick, P. Murray, S. Nesbit, M. Meyer, S.M. Bragg-Sitton, Industry-valued design objectives for advanced LWR fuels and concept screening results, TopFuel 2013, Charlotte, NC, Sep. 15–19, 2013.

[10] S.J. Zinkle, K.A. Terrani, J.C. Gehin, L.J. Ott, L.L. Snead, Accident tolerant fuels for LWRs: a perspective, J. Nucl. Mater. 448 (2014) 374–379.
[11] J. Bischoff, P. Blanpain, J. Strumpell, Development of Fuels with Enhanced Accident Tolerance, IAEA Technical Meeting on Accident Tolerant Fuel Concepts for LWRs, Oak Ridge National Lab, USA, Oct. 13–14, 2015.
[12] A.M. Savchenko, V.B. Ivanov, V.V. Novikov, M.V. Skupov, G.V. Kulakov, V.K. Orlov, O.I. Uferov, Y.V. Konovalov, Review of A.A. BOCHVAR Institute activities in developing potentially accident tolerant fuel for LWRs, TopFuel 2015, American Nuclear Society, Zurich(Switzerland) Sep. 13–17, 2015.
[13] S. Ray, P. Xu, E. Lahoda, L. Hallstadius, F. Boylan, S. Johnson, Westinghouse accident tolerant fuel program—current results & future plans, TopFuel 2015, American Nuclear Society, Zurich(Switzerland) Sep. 13–17, 2015.
[14] T. Liu, Update of accident tolerant fuel R&D status in China, 4th Meeting of the Expert Group on Accident Tolerant Fuels for Light Water Reactors, PSI, Villingen(Switzerland) Sep. 17–18. 2015.
[15] W.-J. Kim, D. Kim, J.Y. Park, Fabrication and material issues for the application of SiC composites to LWR fuel cladding, Nucl. Eng. Technol. 45 (2013) 565–572.
[16] S. Ray, S.C. Johnson, E.J. Lahoda, Preliminary assessment of the performance of SiC based accident tolerant fuel in commercial LWR systems, TopFuel 2013, American Nuclear Society, Charlotte, USA, Sep. 15–19, 2013.
[17] J.H. Yang, K.S. Kim, D.J. Kim, J.H. Kim, J.S. Oh, Y.W. Rhee, Y.H. Koo, Micro-cell UO2 pellets for enhanced accident tolerant fuel, TopFuel 2013, American Nuclear Society, Charlotte, USA, Sep. 15–19, 2013.
[18] D.J. Kim, Y.W. Rhee, J.H. Kim, K.S. Kim, J.S. Oh, J.H. Yang, Y.H. Koo, K.W. Song, Fabrication of micro-cell UO_2–Mo pellet with enhanced thermal conductivity, J. Nucl. Mater. 462 (2015) 289–295.
[19] J.H. Yang, D.J. Kim, K.S. Kim, Y.H. Koo, UO_2–UN composites with enhanced uranium density and thermal conductivity, J. Nucl. Mater. 465 (2015) 509–515.
[20] L.J. Ott, K.R. Robb, D. Wang, Preliminary assessment of accident-tolerant fuels on LWR performance during normal operation and under DB and BDB accident conditions, J. Nucl. Mater. 448 (2014) 520–533.
[21] K.A. Terrani, D. Wang, L.J. Ott, R.O. Montgomery, The effect of fuel thermal conductivity on the behavior of LWR cores during loss-of-coolant accidents,, J. Nucl. Mater. 448 (2014) 512–519.
[22] G. Brillant, F. Gupta, A. Pasturel, Fission products stability in uranium dioxide, J. Nucl. Mater. 412 (2011) 170–176.
[23] D. Jadernas, F. Corleoni, A. Puranen, P. Tejland, M. Granfors, PCI mitigation using fuel additives, TopFuel 2015, American Nuclear Society, Zurich(Switzerland) Sep. 13–17, 2015.
[24] H.S. Lee, D.J. Kim, S.W. Kim, J.H. Yang, Y.H. Koo, D.R. Kim, Thermal conductivity of metallic micro-cell fuel pellet with different unit cell geometry, Spring Meeting 2015, Korean Nuclear Society, Jeju(Korea) May 7–8, 2015.
[25] J.H. Yang, D.J. Kim, K.S. Kim, Y.H. Koo, Thermo-physical property of micro-cell UO2 pellets and high density composite pellets for accident tolerant fuel, IAEA Technical Meeting on Accident Tolerant Fuel Concepts for LWRs, Oak Ridge National Lab., USA, Oct. 13–14, 2015.
[26] D.J. Kim, J.H. Yang, J.H. Kim, K.S. Kim, Y.W. Rhee, J.S. Oh, Y.H. Koo, Metal network containing micro-cell UO2 pellets for accident tolerant fuel, 11th Pacific Rim Conference of Ceramic Societies, Jeju(Korea) Aug. 30–Sept. 4, 2015.
[27] B.J. Lewis, W.T. Thompson, F. Akbari, D. Thompson, C. Thurgood, J. Higgs, Thermodynamic and kinetic modelling of fuel oxidation behaviour in operating defective fuel, J. Nucl. Mater. 328 (2004) 180–196.
[28] J. Spino, P. Peerani, Oxygen stoichiometry shift of irradiated LWR-fuels at high burn-ups: review of data and alternative interpretation of recently published results, J. Nucl. Mater. 375 (2008) 8–25.
[29] D.H. Hwang, S.G. Hong, W.K. In, Evaluation of physical characteristics of PWR cores with accident tolerant fuels, Autumn Meeting 2015, Korean Nuclear Society, Gyeongju(Korea), Oct. 29–30, 2015.
[30] G.J. Youinou, R.S. Sen, Impact of accident-tolerant fuels and claddings on the overall fuel cycle: a preliminary systems analysis, Nucl. Technol. 188 (2014) 123–128.
[31] M. Uno, T. Nishi, M. Takano, Thermodynamic and thermophysical properties of the actinide nitrides, in: Comprehensive Nuclear Materials, Elsevier, 2012, pp. 61–85.
[32] J.M. Harp, P.A. Lessing, R.E. Hoggan, Uranium silicide pellet fabrication by powder metallurgy for accident tolerant fuel evaluation and irradiation, J. Nucl. Mater. 466 (2015) 728–738.
[33] B.J. Jaques, J. Watkins, J.R. Croteau, G.A. Alanko, B. Tyburska-Püschel, M. Meyer, P. Xu, E.J. Lahoda, D.P. Butt, Synthesis and sintering of UN–UO_2 fuel composites, J. Nucl. Mate.r 466 (2015) 745–754.
[34] P.A. Lessing, INL/EXT-12–24974, Oxidation Protection of Uranium Nitride Fuel Using Liquid Phase Sintering, Idaho National Laboratory, 2012.
[35] G.A. Rama Rao, S.K. Mukerjee, V.N. Vaidya, V. Venugopal, D.D. Sood, Oxidation and hydrolysis kinetic studies on UN, J. Nucl. Mater. 185 (1991) 231–241.
[36] K.H. Kim, D.B. Lee, C.K. Kim, G.E. Hofman, K.W. Paik, Characterization U-2wt% Mo and U-10 wt% Mo alloy powders prepared by centrifugal atomization, J. Nucl. Mater. 245 (1997) 179–184.
[37] H.G. Kim, I.H. Kim, Y.I. Jung, D.J. Park, J.Y. Park, Y.H. Koo, Microstructure and mechanical strength of surface ODS treated Zircaloy-4 sheet using laser beam scanning, Nucl. Eng. Technol. 46 (4) (2014) 521–528.
[38] H.G. Kim, I.H. Kim, Y.I. Jung, D.J. Park, J.Y. Park, Y.H. Koo, Adhesion property and high-temperature oxidation behavior of Cr-coated Zircaloy-4 cladding tube prepared by 3D laser coating, J. Nucl. Mater. 465 (2015) 531–539.
[39] L.L. Snead, T. Nozawa, Y. Katoh, T.S. Byun, S. Kondo, D.A. Petti, Handbook on SiC properties for fuel performance modeling, J. Nucl. Mater. 371 (2007) 329–377.
[40] K. Yueh, D. Carpenter, H. Feinroth, Clad in clay, Nucl. Eng. Int. 55 (2010) 14–16.
[41] K.A. Terrani, B.A. Pint, C.M. Parish, C.M. Silva, L.L. Snead, Y. Katoh, Silicon carbide oxidation in steam up to 2 MPa, J. Am. Ceram. Soc. 97 (2014) 2331–2352.
[42] D. Carpenter, An Assessment of Silicon Carbides as a Cladding Material for Light Water Reactors, Ph.D. thesis, Massachusetts Institute of Technology, 2010.
[43] Y. Katoh, L.L. Snead, I. Szlufarska, W.J. Weber, Radiation effects in SiC for nuclear structural applications, Curr. Opin. Solid State Mater. Sci. 16 (2012) 143–152.
[44] D. Kim, H.-G. Lee, J.Y. Park, W.-J. Kim, Fabrication and measurement of hoop strength of SiC triplex tube for nuclear fuel cladding applications, J. Nucl. Mater. 458 (2015) 29–36.
[45] D. Kim, J. Lee, J.Y. Park, W.-J. Kim, Effect of filament winding methods on surface roughness and fiber volume fraction of SiC_f/SiC composite tubes, J. Korean Ceram. Soc. 50 (2013) 359–363.
[46] D.G.S. Davies, The statistical approach to engineering design in ceramics,, Proc. Br. Ceram. Soc. 22 (1973) 429–452.
[47] W.-J. Kim, H.S. Hwang, J.Y. Park, W.-S. Ryu, Corrosion behaviors of sintered and chemically vapor deposited silicon

carbide ceramics in water at 360°C, J. Mater. Sci. Lett. 22 (2003) 581–584.
[48] L. Tan, T.R. Allen, E. Barringer, Effect of microstructure on the corrosion of CVD-SiC exposed to supercritical water, J. Nucl. Mater. 394 (2009) 95–101.
[49] J.-Y. Park, I.-H. Kim, Y.-I. Jung, H.-G. Kim, D.-J. Park, W.-J. Kim, Long-term corrosion behavior of CVD SiC in 360°C water and 400°C steam, J. Nucl. Mater. 433 (2013) 603–607.
[50] C.H. Henager Jr., A.L. Schemer-Kohrn, S.G. Pitman, D.J. Senor, K.J. Geelhood, C.L. Painter, Pitting corrosion in CVD SiC at 300°C in deoxygenated high-purity water, J. Nucl. Mater. 378 (2008) 9–16.
[51] D. Kim, H.-G. Lee, J.Y. Park, J.-Y. Park, W.-J. Kim, Effect of dissolved hydrogen on the corrosion behavior of chemically vapor deposited SiC in a simulated pressurized water reactor environment, Corros. Sci. 98 (2015) 304–309.